ARCHIVES OF METALLURGY

Volume 45 2000 Issue 4

MARIA RICHERT*, ANDRZEJ BACZMAŃSKI**, JAN RICHERT*

MODELLIZATION OF CYCLIC EXTRUSION COMPRESSION USING ELASTOPLASTIC MODEL

MODELOWANIE PROCESU CYKLICZNEGO WYCISKANIA ŚCISKAJĄCEGO (CWS) PRZY UŻYCIU MODELU ELASTOPLASTYCZNEGO

In this work the development of texture and microstructure in the range of very large deformations exerted by the CEC process were studied. The elastoplastic models were used to predict the behaviour of aluminium subjected to the reversible tensile and compressive deformations. The theoretical pole figures well fit to the experimental ones. During the CEC process the texture changes periodically leading to relatively low sample anisotropy for large degree of deformation. The evolution of microstructure was not reversible, however, some parameters (for example hardening) reached the saturation after a few cycles.

W pracy przedstawiono ewolucję tekstury i mikrostruktury w zakresie bardzo dużych odkształceń wywieranych metodą cyklicznego wyciskania ściskającego (CEC). Modele elastoplastyczne zostały użyte do przewidywania zmian tekstury w próbkach aluminiowych poddanych na przemian rozciąganiu i ściskaniu. Stwierdzono dobrą zgodność doświadczalnych i modelowych figur biegunowych. Podczas procesu CWS tekstura zmienia się periodycznie, powodując niską anizotropię materiału w zakresie bardzo dużych odkształceń. Stwierdzono, że ewolucja struktury nie była cykliczna, jednakże pewne parametry materiału (np. umocnienie plastyczne) osiągało stan nasycenia już po kilku cyklach odkształcenia metodą CWS.

1. Introduction

The cyclic extrusion compression (CEC) process [1] introduces reversible flow of metal through the narrowing, in which not only the change of sample diameters,

* WYDZIAŁ METALI NIEŻELAZNYCH, AKADEMIA GÓRNICZO-HUTNICZA, 30-059 KRAKÓW, AL. MICKIEWICZA 30
** WYDZIAŁ FIZYKI I TECHNIKI JĄDROWEJ, AKADEMIA GÓRNICZO-HUTNICZA, 30-059 KRAKÓW, AL. MICKIEWICZA 30

but also the change of the deformation state from compression to elongation occurs [1, 2, 3]. Exerting a very large deformation amplitude, i.e., $\varphi = 0.4 - 0.9$ of the true strain in one cycle, the significant changes in microstructure were involved. The rebuilding of microstructure from microband microstructure to subgrain type microstructure was found [2–9]. With the increase of deformation the increase of microbands density was observed. Above the conventional range of strains ($\varepsilon > 4$) almost the whole volume of samples was filled by the mutually crossed microbands, that caused the formation of characteristic chessboard like microstructure [1–7]. The chessboard like microstructure, in turns, was transformed into almost eqiaxial subgrains microstructure in the range of deformation in which the flow stress was stable [4, 9]. The steady state in mechanical properties was not only connected with the formation of subgrain microstructure, but also with stabilisation of the grain orientation [9]. This stabilisation suggests the repeatable rotation of polycrystalline grains during the reversible flow.

The predictions of Leffers-Wierzbanowski (L-W) [10, 11] and self-consistent [12, 13] deformation models should confirm the texture development in the CEC process. The main aim of the work concerns in the determination of the basic mechanism, leading to the steady state phenomenon in aluminium deformed by the CEC method in the range of very large deformations, considerably exceeding the conventional range of strais.

2. Methods of investigations

2.1. Experimental technique

The investigations were performed on Al99.992 polycrystalline samples with the grain size $\bar{l} = 0.8$ mm, Al99.5 with the grain size $\bar{l} = 2.8$ mm, and AlMg5 polycrystalline samples with the grain $\bar{l} = 0.8$ mm.

The samples were deformed by the cyclic extrusion compression (CEC) method, very useful for obtaining the arbitrarily large plastic deformations, considerably exceeding the conventional range of strais [1]. The total true strain of the n cycles in the CED process can be calculated from the formula:

$$\varepsilon = 4n\varphi = 4n \ln \frac{d_o}{d_m}, \tag{1}$$

where: d_o — is the chamber diameter; d_m — is the die narrowing diameter, n — number of exerted cycles of CEC process and φ — is the deformation applied in one cycle.

It should be emphasised that the cumulated strain is obtained using reversible tensile and compression type of deformation and the real size of the sample does not change after n cycles.

The Al99.992 and Al99.5 samples were deformed with the $\varphi = 0.9$ of true strain in one cycle in the range of true strains from 0.9 to about 60. The AlMg5 samples were deformed in the range of true strains 0.4 – 16 with the strain of $\varphi = 0.4$ in one cycle. Following the deformation the samples had a cylindrical shape. They were cut by means of an electric spark machine along the axis, in the middle of the samples. Then the longitudinal sections were polished. The texture was investigated using the TZ6 texture device, mounted on the IRIS 5 X-ray equipment. Three pole figures of $\{001\}$, $\{011\}$ and $\{111\}$ planes were measured on the longitudinal sections in the middle of the samples, by means of the Schultz's reflection technique.

After the CEC deformation the yield stress of samples was measured in the compression test, performed at the MTS machine with the strain rate of $\dot{\varepsilon} = 2.8 \times 10^{-3} \text{s}^{-1}$.

2.2. Theoretical calculations

The elastoplastic models [10 – 13] were used for simulation of the CEC process consisting of reversible uniaxial tensile and compressive deformation [1, 3]. These models treat the given number of polycrystalline grains having different lattice orientations. The calculations are based on the modelisation of the processes occurring inside and between grains. Using the models the evolution of the microstructure (density of dislocations) and of the anisotropy of grain orientations can be studied. Moreover, the internal stresses for various grain orientations and for the whole sample are predicted.

The deformation models, used in this work, are based on the prediction of the elastoplastic behaviour of a crystal grain inside the polycrystalline material under applied external stress (Σ_{ij}). If the σ_{ij} local stress (at the particular grain) is large enough the plastic deformation occurs due to slip phenomenon. According to the Shmid's law, the slip can be activated only on this slip system $[u\,v\,w]\,(h\,k\,l)$ (the slip direction and plane are specified) for which the resolved shear stress $\sigma_{[uvw](hkl)}$ exceeds some critical value τ_c [10 – 14], i.e.:

$$\sigma_{[uvw](hkl)} \geqslant \tau_c, \tag{2}$$

where: τ_c is the critical shear stress for the slip, $\sigma_{[uvw](hkl)} = \sigma_{ij} m_i n_j$ is the resolved shear stress, $\boldsymbol{n} = [n_1, n_2, n_3]$ is the unit vector normal to the $(h\,k\,l)$ plane and $\boldsymbol{m} = [m_1, m_2, m_3]$ is the unit vector parallel to the $[u\,v\,w]$ direction.

During the plastic deformation, the following physical phenomena influence the mechanical behaviour of the grain [12, 13]:

- multiplication of dislocations and evolution of their spatial distribution inside a grain which lead to the hardening of slip systems (τ_c increases with deformation),
- generation of internal (residual) stresses by plastic incompatibilities,
- changes of crystal orientation of the grain (i.e., a texture formation),
- modification of the grain shape.

To predict the plastic deformation, all the above mentioned processes should be considered at the grain size scale. Moreover, the influence of the macroscopic quantities (Σ_{ij} — macrostresses and E_{ij} — macrostrains) on the behaviour of the grain (σ_{ij}, ε_{ij} local stress and strain) must be established. The above problems are a crucial one for the modelling and it can be solved using some additional assumptions. In this work the two models using different approaches were used.

a) self-consistent (SC) model [12, 13]

Kroner [15] and Hill [16] proposed the principles of the self-consistent model for prediction of elastoplastic deformation. Next, many authors [17–22] have developed the model. Here the calculations have been performed usig the computer program based on the formalism proposed by Berveiller and Zaoui [18] and Lipinski and Berveiller [13].

According to this formalism, the polycrystalline material is approximated by a macro-homogeneous medium at the macroscopic scale and micro-heterogeneous medium at microscopic scale. The ralation between local and global strain and stress rates can be expressed through [12, 13]:

$$\dot{\varepsilon}_{ij} = B_{ijkl}\dot{\Sigma}_{kl}, \tag{3}$$

where: $\boldsymbol{B}$ is the concentration tensor calculated assuming the polycrystalline grain as an ellipsoidal inclusion embedded to the homogeneous matrix and dot means time derivative.

b) Leffers-Wierzbanowski (LW) method [10, 11]

This model is based on that of Leffers [10] and Wierzbanowski [11] but it is enriched with some concepts of the self consistent method. The internal stress, in this model, is proportional to the deference of deformation rates between a current grain and the idealised matrix. The total stress rate $\dot{\sigma}_{ij}^{I}$ "seen" by the grain is [11]:

$$\dot{\sigma}_{ij} = \dot{\Sigma}_{ij} + \alpha\left(\dot{E}_{ij} - \dot{\varepsilon}_{ij}\right), \tag{4}$$

where: α is the factor of elastoplastic accommodation (shape control parameter). The above formula relates the stress and strain rates defined at the macroscopic and the grain size scales, however, the value of α factor is unknown and it has to be a' priori assumed.

3. Results

The cycle of CEC deformation consists of two processes i.e., tensile until the uniaxial strain of $\frac{1}{2}\varphi$ (where φ is the total strain imposed in one cycle) and compression until the same strain. Consequently, the polycrystalline grains rotate

toward the preferred orientations imposed by the two different deformations. Because of the opposite characters of tensile and compression mode, the orientation of crystallites oscillate between two different positions in orientation space. This situation repeats for the next cycles of CEC. After a few cycles, the process of texture transformation is stabilised and the anisotropy of the sample does not increase continously. In the point of view of microstructure the situation is totally different. Such parameters of material as hardness, multiplication of dislocations do not depend on the deformation mode and they continuously increase. The advantage of the CEC method is that after many cycles the microstructure corresponds to extremely large strain, however, the anisotropy of the sample is not very strong.

Fig. 1a shows the $\{111\}$ pole figures of Al99.5 polycrystalline samples with grains of size $\bar{l} = 2.8$ mm, deformed in the range of true strains $\varepsilon = 0.9 - 57.1$. The pole figures for Al99.5 show development of compression texture, measured in the middle of the samples after the compression of samples to its original shape. The origin material, which was annealed before deformation by using the CEC method, shows a lot of separated peaks of intensity, distributed randomly, without preferred orientation (Fig. 1a). Already after one cycle of the CEC process ($\varphi = 0.9$ of true strain) the clear preferred orientation is observed. The development of texture during the CEC deformation leads to the strong axial type of texture, especially after 64 cycles of the CEC deformation ($\varepsilon = 57.1$ of true strain). On the other hand, the large spread around peaks of preferred orientations, in comparison to the origin material, is observed suggesting scattering of orientations. The misorientation between subgrains in samples deformed by using the CEC deformation has been investigated by using the transmission electron microscope and scanning electron microscope technique [8]. The significant increase of misorientation with the increase of deformation has been found. It agrees with the spread of orientation around the peaks of maximal intensity on pole figures.

The experimental pole figures were measured for different samples deformed with different number of CEC cycles. The final texture strongly depends on the initial sample having large randomly orientated grains ($\bar{l} = 2.8$ mm). Especially, for a small number of cycles, when the large grains still remain, the measured pole figures look different because they contain some orientations belonging to the axial texture obtained at very large deformation (for example after 64 cycles of CEC; Fig. 1a). The CEC process is axially symmetrical, therefore it is expected that for all samples, the finally observed preferred orientations belong to the same type of fibre texture. The type of fibre texture should be found if a similar process is simulated by the model and the results are compared with experimental ones. It should be stated that in this comparison only the type of fibre is important because particular orientations are randomly distributed within the fibre. Using the pole figures the fibres can be identified and the detailed analysis of orientations (from ODF) is not necessary.

Using the L-W (Fig. 1b) and self-consistent (Fig. 1c) models the simulation of the texture behaviour was performed. In calculations the constant number of 300 crystallites having random orientations was treated. In the case of L-W model, the

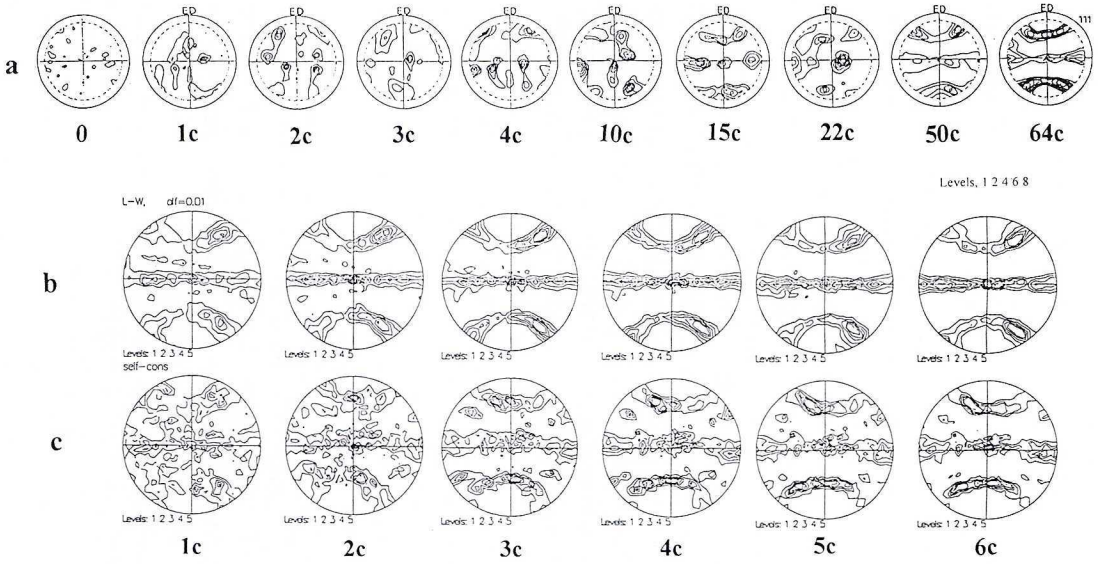

Fig. 1. The (111) experimental pole figures (a) are comapred with the L-W (b) and self consistent models (c) for Al99.95. The texture corresponding to the compressive part of deformation are shown (the number of cycles is indicated and $\varphi = 0.9$ was assumed for a single cycle). For prediction the parameters from Table 1 were used

texture development was predicted with the assumption of factor $\alpha = 0.01$ related to the strong constrains. It agrees with the mode of the CEC deformation, in which the strong compressive stresses are imposed and the sample shape is fully controlled by the tool walls. The other model parameters are shown in Table.

The {001}, {011} and {111} predicted pole figures show the same tendency as pole figures obtained in experiment (for example the {111} pole figures are presented in Fig. 1). The peaks of maximal intensity on the measured pole figures correspond to the fibre texture observed on the predicted figures. Especially for the highest deformations, the results of the self-consistent model agree with the experimental data. The theoretical texture characteristic for compression was obtained much faster than the experimental one (Fig. 1) because the beginning of the CEC process, corresponding to the fragmentation of large grains, cannot be included to the simulation procedure. After a few cycles (presented in Fig. 1 – 3) the texture started to change periodically between two states characteristic for tensile and compression modes.

TABLE 1

Parameters used for the self-consistent and L-W models (where: μ, ν — are the shear and Poisson modulus for Al; τ_o, τ_{sat} — are the initial and the saturation values of critical shear stress, respectively)

	μ(GPa)	ν	τ_o(MPA)	τ_{sat}(MPa)
AlMg5	27.1	0.33	20	130
Al99.5	27.1	0.33	15	43
Al99.992	27.1	0.33	10	24

Fig. 2a and 2b indicate the development of the tensile texture, which could be found in the area of the narrowing of samples deformed by the CEC method, in which the tensile stresses are dominated. The presented pole figures complete the results of compression texture and they suggest reversible character of texture transformation.

In the Fig. 3 the orientation distribution functions (ODF) obtained by self-consistent model for six subsequent cycles of deformation are presented. The cross sections along ϕ_2 axis with step of 5° are shown. The textures are given just after the tensile (Fig. 3a) and compressive (Fig. 3b) part of each cycle. The results are compared with the orientation distribution functions predicted by self-consistent model for simple tensile and compression (Fig. 4). However, in contrast with CEC, the tensile and compressive processes cannot be realised practically for the very large deformations considered in this work.

After tensile mode of CEC process the ODFs consist of the components which belong to the <111> and <100> fibre textures (Fig. 3a). The absolute and relative intensities of the both maximums do not vary significantly with deformation. Similar texture can be found from modelling of simple tensile process (Fig. 4a), however in this case the <100> component relatively decreases in

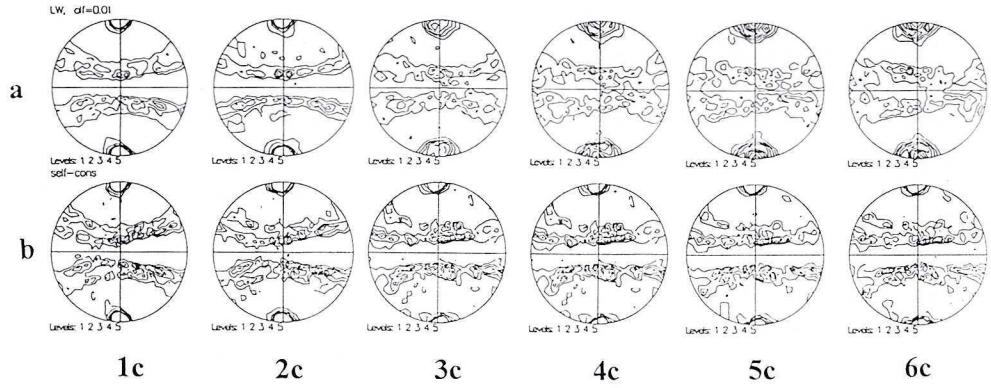

Fig. 2. (111) pole figures predicted by L-W (a) and self-consistent (b) models. The textures corresponding to the tensile part of deformation are shown for six subsequent cycles of CEC process

comparison with $<111>$ for large deformations. Moreover, when the texture develops, some components of the $<111>$ fibre disappear and some of them increase. The last process has a random character, because it cannot be explained by any physical phenomenon in the case of axial symmetry of considered deformation.

After compressive part of CEC process the components near $<110>$ fibre are created (Fig. 3a). In this case, the ODFs maximums are much lower in comparison with those obtained for analogous deformations when the compression process was simulated (Fig. 4a).

The characteristic is that the maximums of ODFs have different positions for compression and tensile deformation and the texture functions are completely rebuilt when the deformation mode is changed. The orientations stable for the both processes were not observed. The ODF functions presented in Fig. 3 confirm the reversible character of texture transformation during the CEC process.

The texture sharpness is quantitatively characterised by the texture index: $I = \int_E f^2(g)\,dg$ [23], where $f(g)$ is the orientation distribution function and g is the orientation. In Fig. 5 the texture indexes after tensile and compressive parts of CEC process are compared with the simple tensile and simple compression respectively (i.e., the comparison was performed always for the same types of texture). It can be concluded that the ODF, after a few cycles of CEC process, is stable (periodical transformation) and it does not changer significantly with deformation. The texture for simple compression or tensile modes develops much faster and it is very sharp in comparison with the CEC process.

As it was mentioned the microstructure of the grains should change continuously in the same direction in spite of the deformation mode (tensile or compression) [1–9]. To prove this assumption the sample hardening was studied. It was shown [24] that the critical shear stress τ_c is changing proportionally with the root square from the density of dislocation and the same dependence should occur for the macroscopic yield stress of the material. Using the self-consistent model (for

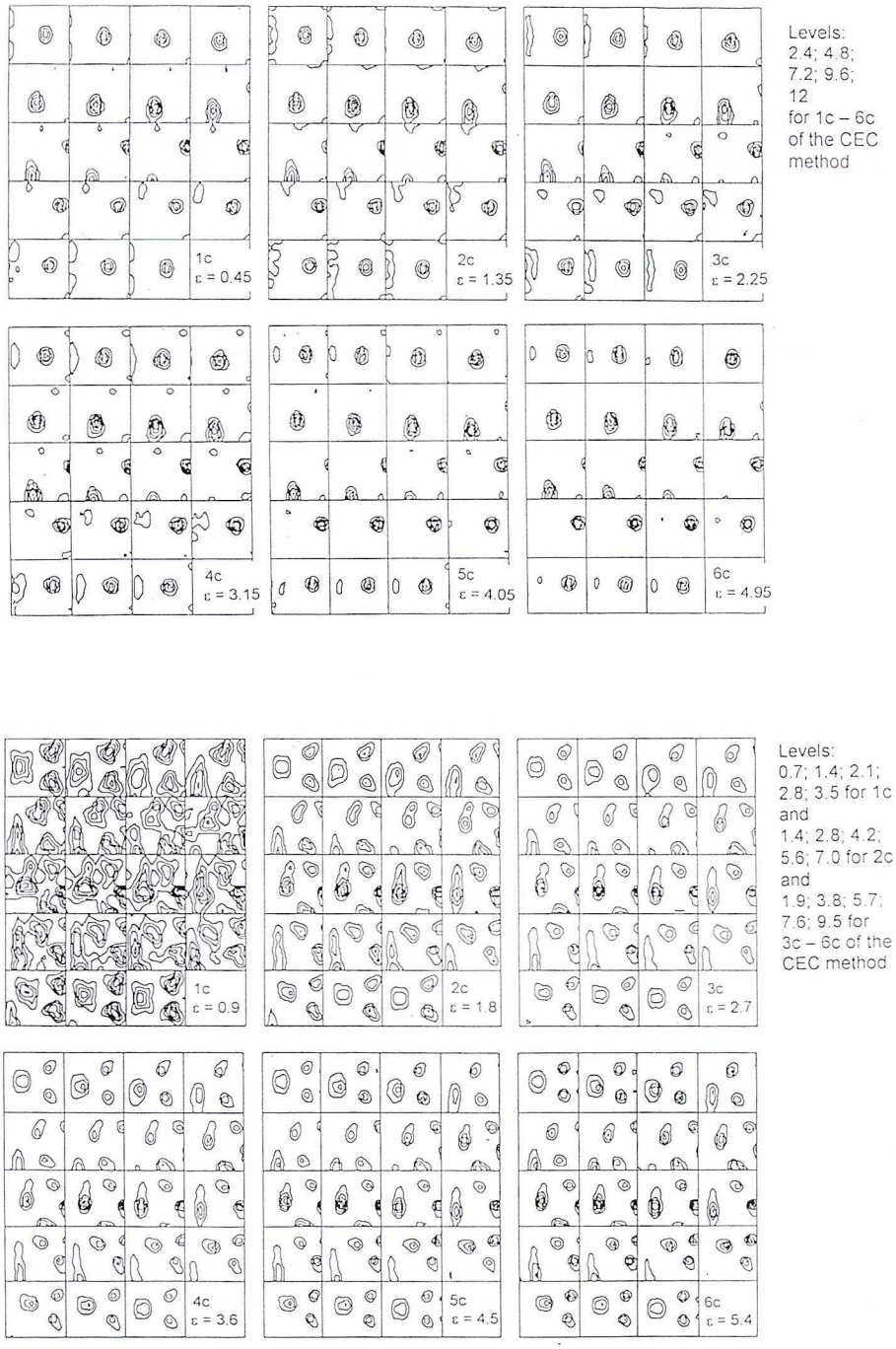

Fig. 3. Theoretical orientation distribution functions (ODFs) predicted by self-consistent model. The cross sections along ϕ_2 axis with step of 5° are shown for six subsequent cycles of CEC process. The textures after tensile (a) and compressive (b) parts of deformations are shown

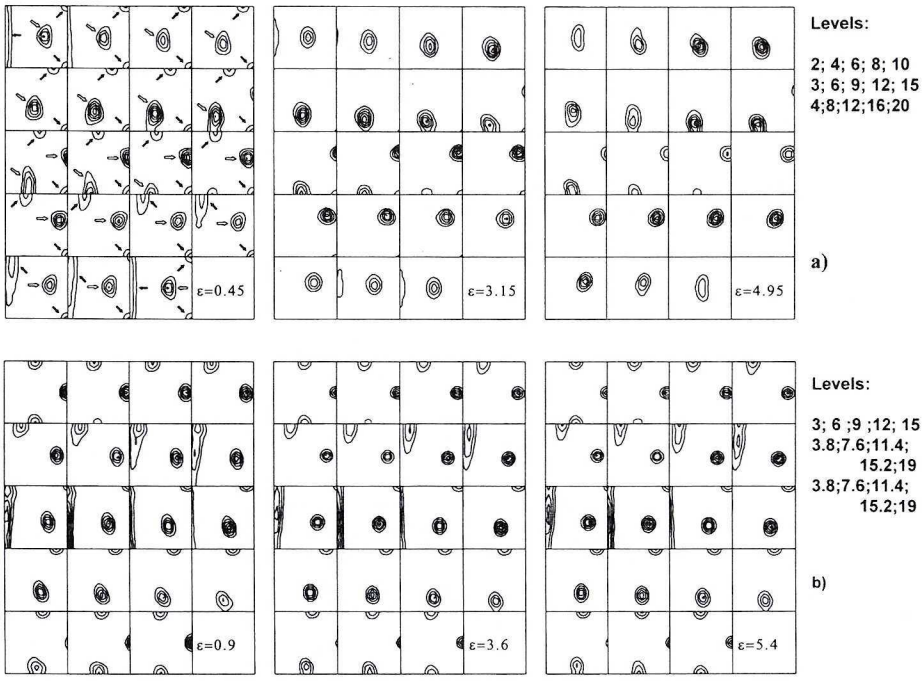

Fig. 4. Theoretical orientation distribution functions (ODFs) predicted by self-consistent model. The cross sections along ϕ_2 axis with step of 5° are shown for: (a) simple tensile (the components of $<111>$ and $<100>$ fibres are indicated by the empty and black arrows, respectively) and (b) simple compression (all component belong to the $<110>$ fibre)

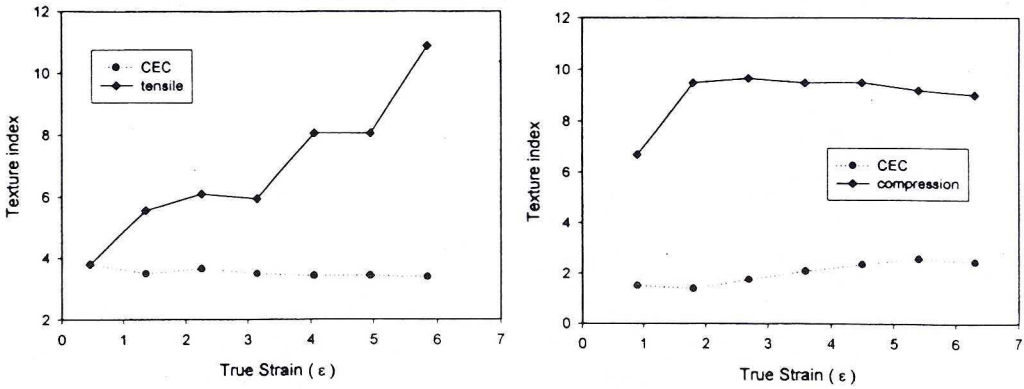

Fig. 5. Evolution of sample anisotropy with deformation. The texture indexes after tensile (a) and compressive (b) parts of CEC process are compared with the simple tensile and simple compression, respectively

parameters given in Table 1) the stress — strain curve was predicted and shown in the Fig. 6. One can see that the hardening of the sample increase progressively with the CEC deformation. The theoretical yield stress (at 0.2% of deformation) is

compared with the experimental one for different samples. The saturation of hardening (and of multiplication of dislocations) started much faster for the pure material than for the alloy.

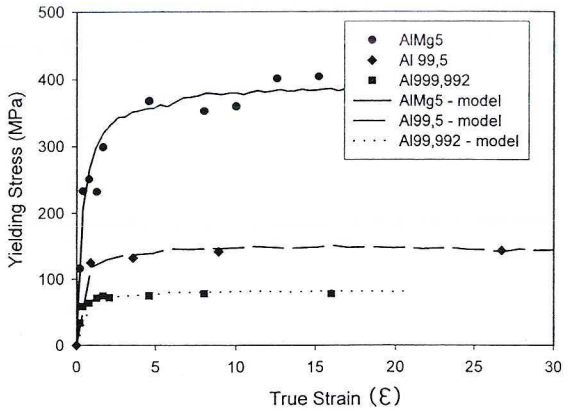

Fig. 6. The yield stress (at 0.2% of deformation) predicted by self-consistent model for parameters given in Table 1 is compared with the experimental values for AlMg5, Al99.5 and Al99.992 samples

General conclusions

1. The obtained results show that very large deformations, more exceeding conventional range of strains, exerted by using the cyclic extrusion compression (CEC) method, lead at the beginning, to the strong scattering of orientation. After this, in the range of unconventional large strains, above 15 cycles of CEC, the strong tendency to the formation of the stable axial — symmetrical texture was found (Figs. 1, 2).

2. The pole figures predicted by the L-W and self-consistent models well fit to the experimental pole figures in spite of some simplification of stress state, which is assumed as axial tensile followed by compressive stress states (Fig. 1). It confirms the results of crystallographic analysis of slip bands development in the Al99.992 monocrystals deformed by the CEC method [3].

3. The opposite character of tensile (in the area of narrowing) and compression deformation (in the area of chambers of the die) in the CEC process leads to the oscillations of grain orientations between different positions in the orientation space. The texture changes periodically and the anisotropy of the sample does not increase continuously (Fig. 5).

4. The microstructure development is not reversible. Such processes as hardening, multiplication of dislocations do not depend on the deformation mode and they continuously proceed in the same direction. However, after a few CEC cycles these parameters reach some saturation (Fig. 6). Using the CEC method the microstructure corresponding to extremely large strain with relatively low texture can be achieved.

Acknowledgment

The authors acknowledge the support of the Polish Committee for Scientific Research, Grant No. 7 T08A 028 14.

REFERENCES

[1] J. Richert, M. Richert, Aluminium **62,** 8, 604 (1986).
[2] M. Richert, A. Korbel, Journal of Materials Processing. Technology **53,** 331 (1995).
[3] M. Richert, Journal of the Mechanical Behaviour of Materials **8,** No. 4, 295 (1997).
[4] M. Richert, IX Conference on Electron Microscopy of Solids, A. Czyrska-Filemonowicz at all. (eds.) 6–9 May, Kraków–Zakopane, Poland, 235 (1996).
[5] M. Richert, A. Korbel, Materials Science & Engineering A **A234–236,** 908 (1997).
[6] M. Richert, H. McQueen, 35th Annual Conference of Metallurgists, H. McQueen at all. (eds.) 25–29 August 1996 — Queen Elizabeth Hotel, Montreal, Quebec, Canada, 15 (1996).
[7] M. Richert, H. McQueen, J. Richert, Canadian Metal. Quart. **37,** 449 (1998).
[8] M. Richert, Q. Liu, N. Hansen, Materials Science & Enginnering **A260,** 275 (1999).
[9] M. Richert, Inżynieria Materiałowa **2,** 59 (1998).
[10] T. Leffers, Phys. Stat. Sol. **25,** 337 (1968).
[11] J. Tarasiuk, K. Wierzbanowski, J. Kuśnierz, Arch. Metall. **38,** 35 (1993).
[12] M. Berveiller, P. Lipinski, Int. Journ. of Pasticity **3,** 162, (1987).
[13] P. Lipinski, M. Berveiller, Int. Journ. of Plasticity **5,** 149, (1989).
[14] P. Franciosi, M. Berveiller, A. Zaoui, Acta Met. **28,** 273 (1980).
[15] E. Kröner, E. Z. Phys. **151,** 504 (1958).
[16] R. Hill, J. Mech. Phys. Solids **13,** 89 (1965).
[17] J. W. Hutchinson, Proc. Roy. Soc. **A319,** 247 (1970).
[18] M. Berveiller, M. Zaoui, A. J. Mech. Phys. Solids **26,** 325 (1979).
[19] G. J. Weng, Int. J. Engng. Sci. **18,** 1385 (1980).
[20] M. Berveiller, A. Zaoui, J. Mech. Phys. Solids **106,** 295 (1984).
[21] R. Hill, J. R. Rice, J. Mech. Phys. Solids. **20,** 401 (1972).
[22] R. Hill, Proc. Roy. Soc. London **A326,** 131 (1972).
[23] H. J. Bunge, Texture Analysis in Materials Sciences, London, Butterwort (1982).
[24] T. Ungar, A. Borbely, Appl. Phys. Lett. **69,** 3173 (1996).

REVIEWED BY: PROF. DR HAB. INŻ. JERZY JURA

Received: 8 September 2000.